

www.acsami.org Research Article

Dual-Functional Nanofiltration Membranes Exhibit Multifaceted Ion Rejection and Antifouling Performance

John R. Hoffman and William A. Phillip*



Cite This: ACS Appl. Mater. Interfaces 2020, 12, 19944-19954



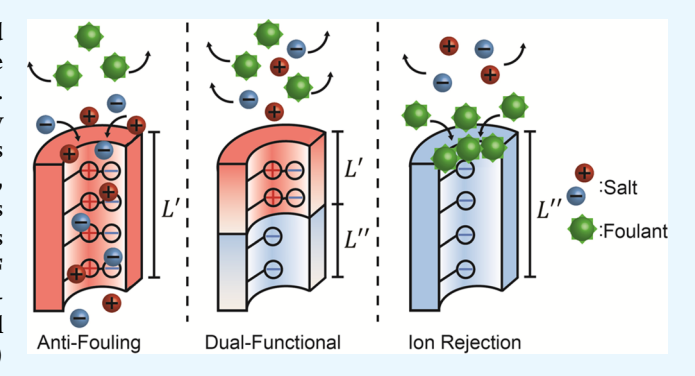
ACCESS

Metrics & More

Article Recommendations

Supporting Information

ABSTRACT: Charged functional groups are often incorporated onto the surface of nanofiltration (NF) membranes to facilitate the selective rejection of multivalent ions over monovalent ions. However, since fouling-resistant surfaces tend to be electrically neutral, the incorporation of charged functionality exacerbates membrane fouling. Multifunctional Janus membrane architectures, which incorporate chemically distinct domains over their cross section, provide a strategy for balancing the competing demands associated with making fouling-resistant, ion rejecting NF membranes. Here, through the controlled exposure of poly-(trifluoroethyl methacrylate-co-oligo-(ethylene glycol) methyl ether methacrylate-co-(3-azido-2-hydroxypropyl methacrylate)) copolymer substrates to a series of reactive solutions containing



alkyne-terminated molecules, the process for creating dual-functional membranes by using the copper(I)-catalyzed azide—alkyne cycloaddition (CuAAC) reaction was analyzed. Under the appropriate conditions, the CuAAC reaction propagates into the copolymer substrate as a front. This phenomenon results in a process for creating layered domains of distinct functionality whereby the distribution of antifouling zwitterionic moieties and ion rejecting sulfonate moieties can be modified by manipulating the exposure time. The ion rejection and fouling propensity for a family of dual-functional membranes was examined. For short initial reaction times, which introduced a thin antifouling layer on top of an ion rejection layer, the rejection of 1 mM K₂SO₄, 87%, was comparable to the value for full charge control membranes, 90%. Moreover, when exposed to a fouling solution containing bovine serum albumin (BSA), these dual-functional membranes exhibited an 18% decline in normalized flux and recovered 99% of their flux upon rinsing with water. In comparison, the full charge membranes exhibited a 44% decline in normalized flux and recovered 65% of their flux upon washing. As such, the results demonstrate that the controlled functionalization process reported here is capable of balancing antifouling and ion rejection capabilities. Furthermore, the versatile nature of the click chemistry mechanism at the center of this process offers a means by which to design and fabricate multifunctional membranes for numerous future applications.

KEYWORDS: nanostructured copolymers, CuAAC click reaction, anti-fouling, bovine serum albumin, nanofiltration membranes

1. INTRODUCTION

Designing effective membrane processes often requires considering how to balance competing material properties to enhance system scale performance. A familiar example of this consideration in membrane separations is the permeabilityselectivity trade-off² where improvements in throughput are often contrasted by a reduced ability to resolve two differing solutes, or vice versa.^{3,4} Despite structural advances that are pushing the limits of the upper bound established by the permeability-selectivity trade-off,5 there remains a need for more selective separation processes. This demand is driving an interest in membrane architectures with controlled chemical functionality.6 In these instances, too, the design of the introduced chemical functionality and the competing material characteristics it can engender must be considered. For example, while the chosen chemistry can lead to the emergence of new, potentially beneficial transport properties, it may also

exacerbate detrimental processes, such as fouling. As such, there is a need to develop methods for introducing chemical functionality in a manner that maximizes its effectiveness while mitigating its adverse effects.

Nanofiltration (NF) membranes provide a useful example of the need to balance competing material characteristics. NF membranes can selectively reject multivalent co-ions (i.e., those with the same charge as the membrane), providing a complementary desalination process to reverse osmosis (e.g., in water softening applications).

Received: February 17, 2020 Accepted: April 7, 2020 Published: April 7, 2020





is often realized through the incorporation of charged functional groups. While the electrostatic repulsion between the charged membrane and co-ions offers the ability to mediate ion rejection, the electrostatic attraction between the membrane and counterion solutes can increase the fouling propensity of the membrane. During fouling, attractive electrostatic, dispersive, and hydrodynamic forces cause solutes such as proteins and humic acids to adsorb to the membrane surface, resulting in pore blockage, pore constriction, and cake layer formation. 10 This accumulation of material lowers the permeability of the membrane and the chemical cleaning needed to restore performance greatly reduces membrane life span. Because of its prevalence, fouling has been examined in detail, and a series of design rules for surfaces that can help reduce fouling propensity have been established. Namely, antifouling surface chemistries (e.g., poly(ethylene glycol) brushes, 11 zwitterionic moieties, 12 and many others 13) tend to exhibit hydrophilic and overall neutral charge characteristics.¹ The need to utilize an overall neutral charge to resist fouling directly contrasts the need for charged moieties to increase ion rejection through a Donnan exclusion mechanism.

Inspired by Janus membranes, the development of dualfunctional NF membranes that consist of an antifouling layer situated above a charge-functionalized, ion rejecting layer may provide one approach to balancing these competing materials properties. Janus membranes, which are characterized by opposing surfaces that possess distinct, asymmetric properties, 15 are an intriguing example of multifunctional membranes that possess unique chemistries distributed over their structure. The manner in which the chemistries on the antipodal surfaces of the Janus membranes interact can be designed to influence their transport properties. ¹⁶ For example, these membranes have been utilized to facilitate the unidirectional transport of water, ¹⁷ separate oil from water, ^{18–20} purify water using nanofiltration, ^{21,22} membrane distillation, ^{23,24} and forward osmosis²⁵ as well as act as membrane separators in batteries.^{26–28} Several processes have been proposed for the fabrication of Janus membranes, ^{15,16} including cocasting ²⁹ and sequential spray methods. ³⁰ Dopamine-based casting techniques³¹ have proven to be useful in both the flat sheet and hollow fiber geometries.³² Unfortunately, the inclusion of the dopamine layers often affects the pore size of membranes in the NF and ultrafiltration (UF) range and alters their transport properties.³³ On the lab scale, advanced vapor deposition techniques^{34,35} as well as a gas backflow assisted apparatus³⁶ have been shown to maintain pore size. With regard to all of these techniques, control over the thickness and distribution of the functionalities that span the membrane cross-section is a critical design consideration to maximize performance in target applications. 16 One example where this need to control functionality is readily evident is the use of Janus membranes as water diodes. In this application, it is believed that the novel behavior that emerges is a result of phenomena that occur at the interface between the hydrophobic and hydrophilic sections of the membrane. Additionally, experiments have demonstrated that reducing the thickness of the hydrophobic section reduced the transmembrane pressure needed to drive transport, while changes to the thickness of the hydrophilic section did not alter the required pressure. 15 As such, additional research is needed to develop fabrication methods that realize the robust formation of multifunctional Janus membranes with controlled nanostructures.

The copper(I)-catalyzed, azide—alkyne cycloaddition (CuAAC) "click" reaction offers a promising technique for addressing the challenges associated with the fabrication of Janus membranes. Since their initial development,³⁷ numerous applications have been designed around the use of these rapid and precise click reaction mechanisms.³⁸ In regards to the functionalization of membranes, the fast rate of the reactions allows for the targeted introduction of chemical functionality. For example, the CuAAC reaction has been utilized to control the functionalization of azide-lined, track-etched pores via the electrochemical generation and diffusion of catalytically active Cu(I) ions.³⁹ In another example, the formulation and deposition of a reactive solution containing alkyne-terminated molecules on the membrane surface has been demonstrated to be a ready method for controlling the functionalization of membranes with exposed azide moieties lining the pore wall. Namely, in the appropriate limit the diffusion of reactive alkynes to exposed azide groups determines the rate of the CuAAC process which empowers controlled conversion through specific exposure times. 40

In this study, membranes derived from a poly(trifluoroethyl methacrylate-co-oligo-(ethylene glycol) methyl ether methacrylate-co-(3-azide-2-hydroxypropyl methacrylate)) [P(TFEMA-OEGMA-AHPMA)] copolymer act as a platform for the generation of multifunctional Janus membranes. Specifically, the azide groups of the AHPMA repeat units provide a handle for the postfabrication functionalization of the mesoporous membranes utilizing the CuAAC reaction mechanism. To investigate the potential the CuAAC process can offer, a multifunctional nanofiltration (NF) membrane with opposing foulant resistant and ion rejecting layers will be examined. The process for creating the dual-functional membranes by first introducing a top layer of antifouling functionality at varied depths into a membrane thickness followed by an additional CuAAC reaction to incorporate charge selective functional groups beneath the antifouling moieties will be investigated. The distribution of the two distinct functional groups over the membrane thickness will be probed by using Fourier transform infrared (FTIR) and scanning electron microscopy—energy dispersive X-ray (SEM— EDX) spectroscopy. Moreover, the impact of this distribution on the hydraulic permeability, pore size, ion rejection performance, and bovine serum albumin (BSA) fouling propensity of the dual-functional membranes will be examined and compared with that of control membranes possessing full charge and full zwitterionic functionality. It is hypothesized that by developing a process that balances the distribution of the two functional groups appropriately, dual-functional membranes with performance simultaneously equivalent to the ion rejecting capabilities of the full charge and fouling resistance of the full zwitterionic control samples can be realized. As such, this process offers the potential for a rapid and viable method for the creation of multifunctional NF membranes.

2. MATERIALS AND METHODS

2.1. Materials. All chemicals were purchased from Sigma-Aldrich unless noted otherwise. Trifluoroethyl methacrylate, oligo(ethylene glycol) methyl ether methacrylate ($M_{\rm n}=500~{\rm g~mol}^{-1}$), and glycidyl methacrylate were purified by passing them through a basic alumina (VWR, West Chester, PA) column prior to use. Deionized water (DI water), used in the preparation of all aqueous solutions for permeability, fouling, and solute rejection tests and for rinsing the

stirred cell at the conclusion of an experiment, was obtained from a Millipore water purification system (Milli-Q Advantage A10, Milli-Q, Billerica, MA). A commercial poly(vinylidene fluoride) (PVDF) ultrafiltration membrane (Nanostone Water, Inc., PV400 ultrafiltration membrane) was used as a support in the membrane casting process.

2.2. Polymer Synthesis and Characterization. A poly-(trifluoroethyl methacrylate-*co*-oligo(ethylene glycol) methyl ether methacrylate-*co*-glycidyl methacrylate) [P(TFEMA-OEGMA-GMA)] copolymer was synthesized by using a free radical polymerization mechanism (see the Supporting Information for details). An epoxide ring-opening reaction with sodium azide resulted in the formation of the poly(trifluoroethyl methacrylate-*co*-oligo(ethylene glycol) methyl ether methacrylate-*co*-(3-azido-2-hydroxypropyl methacrylate)) [P-(TFEMA-OEGMA-AHPMA)] copolymer. The chemical structure and composition of the copolymer were confirmed by using ¹H nuclear magnetic resonance (¹H NMR) spectroscopy (Bruker Avance III HD400) (Figure S1). Deuterated dimethyl sulfoxide was used as the solvent.

2.3. Membrane Fabrication and Functionalization. Parent membranes were fabricated from the P(TFEMA-OEGMA-AHPMA) copolymer using a nonsolvent-induced phase separation (NIPS) method (see the Supporting Information for details). The P(TFEMA-OEGMA-AHPMA) membranes were stored in DI water until further use.

Copper(I)-catalyzed azide-alkyne cycloaddition (CuAAC) "click" reactions were utilized to synthesize the dual-functional membrane structure. The formation of the zwitterionic, antifouling layer was initiated by reacting the parent membrane with 3-(dimethylamino)-1propyne. A reactive solution containing 250 mM 3-(dimethylamino)-1-propyne, 80 mM copper(II) sulfate pentahydrate, and 240 mM ascorbic acid was exposed to an unreacted P(TFEMA-OEGMA-AHPMA) membrane for 0, 5, 10, 20, 30, or 60 s by placing the parent membrane at the bottom of an Amicon stirred cell and filling the reservoir on top with the reactive solution. After the allotted time, the solution was removed and the reservoir was rinsed with DI water and then filled with a 10 mM ethylenediaminetetraacetic acid (EDTA) solution. The EDTA solution was passed through the membrane at an applied pressure of 4.14 bar (60 psi), and 2 mL of solution was collected to remove any bound copper from the porous structure of the membrane. The EDTA solution was then removed and replaced with DI water; 2 mL of DI water was passed through the membrane. The membranes were removed from the stirred cell and then submerged in a 60 mM 1,3-propane sultone solution for 2 h at room temperature. The quaternization reaction between the terminal dimethylamine and sultone creates the zwitterionic functionality. The membranes were then rinsed and stored in DI water.

The zwitterion-functionalized P(TFEMA-OEGMA-AHPMA) membranes were used for the subsequent formation of the charge-functionalized layer. The zwitterion-functionalized membranes were exposed to a reactive solution containing 250 mM propargylamine, 80 mM copper(II) sulfate pentahydrate, and 240 mM ascorbic acid for 5 min to ensure conversion of the remaining azide moieties within the membranes. This reaction was performed by using the Amicon stirred cell in a similar manner to the process detailed for the previous reaction. After rinsing with an EDTA solution and DI water, the membranes were submerged in a 60 mM 4-sulfophenyl isothiocyanate solution for 4 h at 60 °C. These now dual-functional membranes were then rinsed a final time and stored in DI water.

2.4. FTIR Characterization. A Jasco 6300 Fourier transform infrared (FTIR) spectrometer was used for analysis. Each membrane sample was scanned 25 times per measurement over a range of wavenumbers from 650 to 4000 cm⁻¹. Conversion of the azide moieties was monitored by using the decrease in intensity of the peak at 2100 cm⁻¹ along with the formation of peaks associated with the coupled functionality. All spectra were normalized by using the carbonyl peak at 1725 cm⁻¹, which is present within the backbone of the parent copolymer and remains unaffected throughout the CuAAC reaction process.

2.5. SEM-EDX Elemental Mapping. A Magellen 400 scanning electron microscope (SEM) combined with a Bruker Energy dispersive X-ray spectrometer (EDX) was used for analyzing the progression of the reactive 3-(dimethylamino)-1-propyne front into the membrane. Dual-functional membranes were generated by reacting parent membranes with a 3-(dimethylamino)-1-propyne reactive solution for 10, 20, 30, and 40 s, rinsing the membrane with excess 10 mM EDTA solution and DI water, and then reacting the dimethylamine-functionalized membranes with a propargyl chloride solution. Elemental analysis of chlorine was used to monitor the ability to manipulate the penetration depth of the reactive front of 3-(dimethylamino)-1-propyne. Cross-sectional samples for SEM-EDX analysis were prepared by using liquid nitrogen. The membrane was submerged in liquid nitrogen for 15 s and then fractured with tweezers to obtain a smooth cross section. SEM-EDX micrographs and elemental maps were obtained by using a current of 0.8 nA and an accelerating voltage of 15 kV.

2.6. Transport Tests and Fouling Experiments. One-inch-diameter sections of the membranes were punched out by using a circular hole punch and placed in a 10 mL Amicon 8010 stirred cell (Millipore) with the copolymer selective layer facing up. The cell was filled with 10 mL of DI water and pressurized with nitrogen gas to measure the water flux. The water that permeated through the membrane was collected in a 20 mL scintillation vial that rested on a balance. The steady-state water flux at each applied pressure was calculated by measuring the mass of the permeate solution as a function of time. The variation of the water flux over a range of applied pressures from 1.38 to 4.14 bar (20 to 60 psi) was used to calculate the hydraulic permeability.

For neutral solute rejection tests, the membranes were subjected to feed solutions containing 1 g L $^{-1}$ poly(ethylene oxide) (PEO) with molar masses of 1.1, 2.1, 4.0, 6.0, and 9.8 kg mol $^{-1}$ (Polymer Source Inc., Montreal, QC). The dispersity, \mathcal{D}_{1} , of the PEO samples was <1.10. The cell was stirred at 300 rpm to mitigate the effects of concentration polarization. The volume of solution within the stirred cell was maintained at 10 mL throughout the experiments through the continuous addition of solution from an attached reservoir. The stirred cell was rinsed thoroughly with DI water between each experiment. Samples of the feed and permeate solutions were stored at 6 $^{\circ}$ C until the concentrations of PEO in solution were measured by using a Shimadzu TOC-TN organic carbon analyzer. The rejection values reported from these experiments were calculated as follows:

$$R \ (\%) = \left(1 - \frac{C_p}{C_f}\right) \times 100$$
 (1)

where C_p represents the concentration of solute in the permeate solution and C_f represents the concentration of solute in the feed solution. Error bars for this data indicate one standard deviation from multiple experiments (n = 2) on a single membrane.

Ion rejection experiments were executed and analyzed in a similar manner. Feed solutions containing either potassium chloride, KCl, or potassium sulfate, K_2SO_4 , dissolved in DI water at a concentration of 1 or 10 mM were utilized. The pH of these solutions were unadjusted. The concentration of salt in the feed and permeate solutions were determined by using inductively coupled plasma optical emission spectroscopy (ICP-OES) (PerkinElmer Optima 8000) to quantify the elemental concentration of K^+ . The rejection values were reported by using eq 1. Error bars for this data indicate one standard deviation from multiple experiments (n=2) on two membranes of each type.

Membrane fouling was analyzed by subjecting the functionalized membranes to a bovine serum albumin (BSA) solution and quantifying the flux decline as a function of time. Three salt concentrations, 1, 10, and 100 mM sodium chloride, NaCl, and two solution pH values, 3 and 4.7, were used with a 0.5 g $\rm L^{-1}$ BSA solution. The solution pH was adjusted by using 1 M hydrochloric acid, HCl. Prior to each fouling test, a pH adjusted, aqueous solution containing only the background salt was filtered through the membrane until the flux remained stable at a value of 5 L m $^{-2}$ h $^{-1}$ for 5 h. Based on small variations in the membrane permeability, an

applied pressure between 1.24 and 2.06 bar (18 and 30 psi) was used to achieve this initial flux. Subsequently, a 0.5 g L $^{-1}$ of BSA was then dissolved into solution and passed though the membrane for a period of 40 h, at the same applied pressure. Over the 40 h period, depending upon the extent of flux decline observed, 75–125 mL of the fouling solution would permeate through the membrane. Because of the complete rejection of BSA by the copolymer membranes, the final concentration in the stirred cell would increase $\sim\!10\times$ to 5.0 g L $^{-1}$. The fouling propensity was quantified by using a normalized flux, calculated as follows:

normalized flux (%) =
$$\left(\frac{I_i}{I_0}\right) \times 100$$
 (2)

where J_0 is the steady-state flux prior to introducing the BSA foulant, 5 L m⁻² h⁻¹, and J_i is the flux recorded at every hour (i = 1-40) of the fouling experiment. Flux decline is reported as the final normalized flux after 40 h.

Afterward, the membranes were rinsed with fresh DI water, in which the stirred cell was filled and emptied with 10 mL of DI water a total of five times. The stirred cell was filled with 10 mL of DI water and allowed to stir for 1 h without an applied pressure, before being emptied and rinsed again with DI water. The hydraulic permeability of DI water was then quantified to determine the extent of irreversible fouling. Flux recovery is reported as the normalized flux at the end of the rinsing procedure. The fouling results for one of each membrane are discussed below.

3. RESULTS AND DISCUSSION

3.1. Fabrication of Multifunctional Membranes. P-(TFEMA-OEGMA-AHPMA) membranes were cast by using a nonsolvent-induced phase separation (NIPS) method.⁴¹ Upon casting, the microphase separation of the hydrophobic TFEMA backbone from the hydrophilic OEGMA side chains results in a porous membrane structure with azide moieties from the AHPMA repeat units lining the pore walls. Postfabrication, these moieties are functionalized by using the copper(I)catalyzed azide-alkyne cycloaddition (CuAAC) reaction mechanism. The concentration of the alkyne-copper complex in the reactive solution controls the rate of this reaction. 40 Notably, at excess alkyne-copper complex concentrations relative to the azide moieties within the membrane, the reaction rate becomes much faster than the rate of diffusion. These conditions result in a reactive front of alkyne-terminated molecules diffusing into the membrane and rapidly consuming the exposed azide moieties they encounter. Multifunctional membranes can be generated by controlling the penetration depth of this propagating reaction front. Here, for example, the process for creating a dual-functional membrane by manipulating the exposure time to a series of reactive solutions is shown schematically in Figure 1.

An initial reaction with a solution containing 3-(dimethy-lamino)-1-propyne for varying lengths of time results in varied penetration depths, shown as L', with small depths resulting from short exposure times and complete conversion across the membrane cross section occurring at longer times. A quaternization reaction between the terminal dimethylamine and 1,3-propane sultone forms zwitterionic moieties that generate the antifouling functionality within the top layer of the dual-functional membrane. Subsequently, as shown in Figure 1C, the charge-functionalized layer was formed by exposing the membrane to a propargylamine solution for 5 min to consume the azide moieties remaining on the trailing side of the membrane, L''. While this reaction can result in a net positive charge due to the presence of the protonated amine, 42

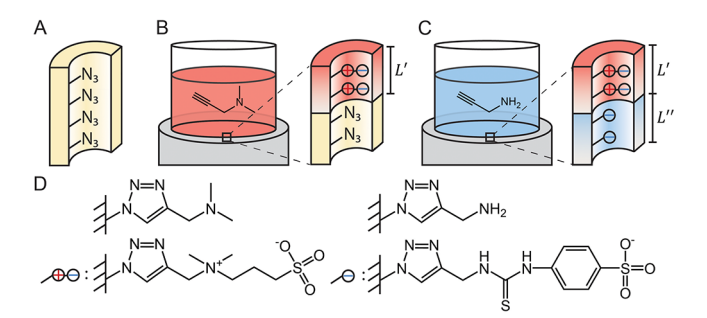


Figure 1. Schematic of the dual-functionalization process. (A) The pore walls of the unreacted membrane are lined by exposed azide moieties. (B) The membrane is placed at the bottom of a stirred cell, and the upper reservoir is filled with a 3-(dimethylamino)-1-propyne reactive solution. Diffusion of the reactive solution over a controlled exposure time results in the conversion of the azide moieties within a depth, L', to dimethylamino moieties that are then functionalized to antifouling zwitterions. (C) Upon rinsing, a second, propargylamine reactive solution is placed within the cell to functionalize the underlying azide moieties within the region, L'', which are further functionalized to negatively charged sulfonate groups. (D) The molecular structures of the initial 3-(dimethylamino)-1-propyne and propargylamine reacted moieties and the subsequent zwitterionic and negatively charged functional groups are depicted.

negative charge functionality was generated by reacting the amine with 4-sulfophenyl isothiocyanate. Compared with the pH-responsive primary amine group, the sulfonate group induces negative charge that is not a strong function of pH over typical operating ranges. 42

3.2. Monitoring Penetration Depth and Conversion of the Functionalization Reactions. The penetration depth of the 3-(dimethylamino)-1-propyne reaction front, L', was monitored using a combination of ATR-FTIR and EDX spectroscopy. Upon exposing the parent membrane to a 3-(dimethylamino)-1-propyne solution, the pore lining azide moieties react to form a 1,2,3-triazole. As shown in Figure 2A, this reaction causes the intensity of the peak at 2100 cm⁻¹ in the FTIR spectra, which is associated with the azide group, to decrease. For short reaction times, 10 s, the azide peak is not completely removed from the FTIR spectrum, indicating that not all the azide moieties within the detectable depth of the FTIR spectrophotometer have reacted. Longer reaction times, >20 s, see full removal of the azide peak along with the more prominent appearance of a peak corresponding to a terminal amine bond at 1630 cm⁻¹.

SEM-EDX elemental maps permit the progression of the 3-(dimethylamino)-1-propyne reactive front to be visualized. For the samples reported in Figure 2B, after the initial reaction with 3-(dimethylamino)-1-propyne, the membranes were exposed to a reactive solution containing propargyl chloride to consume the underlying azide moieties and covalently attach a chlorine atom to the pore wall. Because there is no chlorine in the parent membrane, the chlorine atom provides a distinct signal in the EDX elemental maps to enable visualization. As the exposure time of the 3-(dimethylamino)-1-propyne reaction increased from 10 to 20 to 30 s, it becomes clear that the chlorine intensity on the leading side of the membrane decreases. For the 30 and 40 s samples, the chlorine intensity at the leading edge is consistent with the intensity of an unreacted sample (Figure S2). This observation can be attributed to the azide moieties already having reacted with 3-(dimethylamino)-1-propyne, thereby preventing the

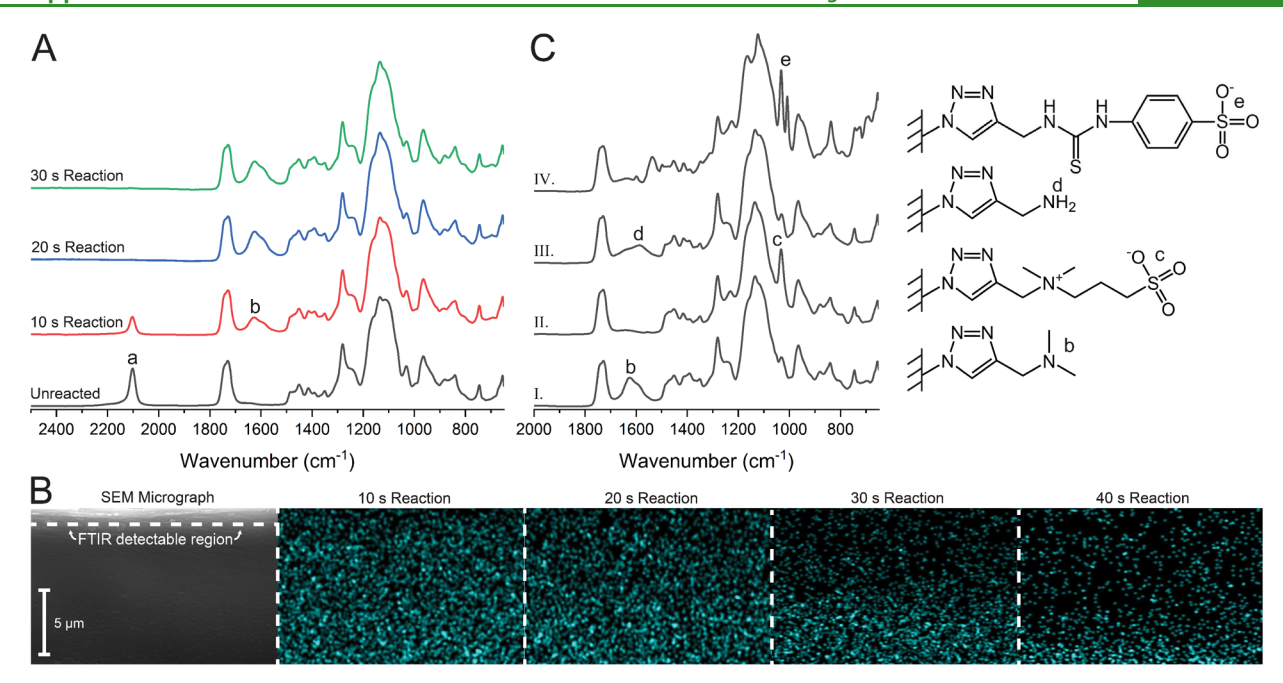


Figure 2. Monitoring the extent of functionalization via FTIR and SEM-EDX. (A) The parent P(TFEMA-OEGMA-AHPMA) copolymer exhibits a characteristic azide peak at 2100 cm^{-1} , labeled a. Exposure to a 3-(dimethylamino)-1-propyne solution results in a decrease in the intensity of this peak. The tertiary amine formed by this reaction generates a peak at 1640 cm^{-1} , labeled b. (B) The progression of the reactive front associated with the 3-(dimethylamino)-1-propyne functionalization process was analyzed by using SEM-EDX to produce elemental maps of chlorine. Membranes were reacted with a 3-(dimethylamino)-1-propyne solution for times that varied from 10 to 40 s, followed by a 300 s exposure to a propargyl chloride reactive solution. The propargyl chloride reacts with azide groups not consumed by the initial reaction. The reactive solutions were deposited on the top surface of the membranes. Scale bars correspond to 5 μ m. (C) Zwitterionic functionality was introduced by exposing the dimethylamino-functionalized membrane to a 1,3-propane sultone solution. This process is characterized by the removal of peak b in spectrum I and the formation of the sulfonic acid peak at ~1030 cm⁻¹, labeled c in spectrum II. Negatively charged functionality was introduced through a propargylamine group, which forms a peak associated with N–H bending at 1580 cm⁻¹, labeled d in spectrum III. Negative charge was incorporated upon exposing the amine-functionalized sample to 4-sulfophenyl isothiocyanate, forming the sulfonic acid group peaks at ~1033 cm⁻¹, labeled e in spectrum IV.

subsequent reaction with propargyl chloride. Notably, the time when the azide peak in the FTIR spectra is fully removed, i.e., 20 s, corresponds well with the sample where the reactive front moved beyond the depth from which the FTIR signal is detected. These observations are consistent with two separate domains of functionality being developed over the membrane cross section. Complete SEM—EDX cross sections (Figure S2) and line spectrum analysis (Figure S3) for all membranes are included in the Supporting Information.

After demonstrating that the penetration depth of the 3-(dimethylamino)-1-propyne reaction can be controlled, we examined the reaction for introducing antifouling zwitterionic functionality using FTIR spectroscopy (Figure 2C). Upon exposure of a dimethylamino-functionalized membrane to a 1,3-propane sultone solution, the 1630 cm⁻¹ peak that is present in spectrum I of Figure 2C disappears and the sulfonate peak at 1030 cm⁻¹ appears in spectrum II, suggesting that the desired zwitterion is formed.

A similar process was used to demonstrate the introduction of the charge-functionalized moieties. Beginning with an unreacted P(TFEMA-OEGMA-AHPMA) membrane, a CuAAC reaction with propargylamine results in the disappearance of the peak associated with azide groups and the formation of a primary amine peak at 1580 cm⁻¹ as shown in spectrum III of Figure 2C. Finally, the negatively charged functionality was formed by reacting this membrane with 4-sulfophenyl isothiocyanate. The double peak at 1030 cm⁻¹ in spectrum IV is associated with thiourea and sulfonic acid

groups that are consistent with the conversion of the terminal amine to the negatively charged sulfonic acid moiety.

Full charge (FC) functionalized, full zwitterionic (FZ) functionalized, and four dual-functional (DF) membranes were made and analyzed in this work. The FC membrane was formed using a 3-(dimethylamino)-1-propyne reaction time of 0 s. The FZ membrane was formed by using a 3-(dimethylamino)-1-propyne reaction time of 60 s. The four DF membranes consisted of initial 3-(dimethylamino)-1-propyne reaction times of 5, 10, 20, and 30 s. These membranes are herein termed 5 DF, 10 DF, 20 DF, and 30 DF, respectively.

The hydraulic permeability of the unreacted parent and functionalized membranes was determined by using dead-end stirred cell experiments. The water flux of each membrane was quantified over applied pressures ranging between 1.38 and 4.14 bar (20 and 60 psi); the hydraulic permeability is equal to the slope of this data (Figure 3A). The parent P(TFEMA-OEGMA-AHPMA) membranes had a permeability of 1.4 \pm 0.3 L m⁻² h⁻¹ bar⁻¹. Upon functionalization, the hydraulic permeabilities for the FZ, FC, and DF membranes rose to an average value of 3.1 \pm 0.2 L m⁻² h⁻¹ bar⁻¹. Regression lines

3.3. Quantifying Membrane Transport Properties.

Neutral solute rejection experiments were performed to examine whether this increase in hydraulic permeability was a result of the functionalization processes disrupting the pore

obtained by fitting water flux measurements are shown in

Figure S4.

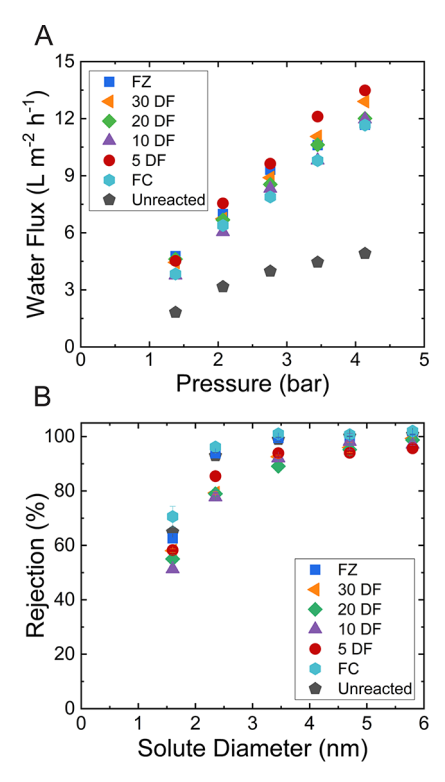


Figure 3. Transport tests for unreacted, full zwitterionic (FZ), 30, 20, 10, and 5 s dual-functional (DF), and full charge (FC) membranes. (A) Water flux vs applied pressure for the copolymer membranes. The hydraulic permeabilities of the membranes were determined from the slope of the data. (B) Solute rejection curves for the copolymer membranes. Poly(ethylene oxide) (PEO) molecules of known size were used as neutral solutes. Feed solutions were made by dissolving PEO samples with molar masses of 1.1, 2.1, 4.0, 6.0, and 9.8 kg mol⁻¹ in DI water. The percent rejection was determined by taking the ratio of the PEO concentration in the permeate solution to the 1 g L⁻¹ feed solution. PEO concentrations were measured by using total organic carbon analysis.

structure of the membranes. Poly(ethylene oxide) (PEO) molecules of varied molar masses from 1.1 to 9.8 kg mol⁻¹, whose hydrodynamic size could be calculated by using literature data, 43 were used in these experiments. Figure 3B shows the percent rejection as a function of solute size. The rapid decline in rejection for PEO samples with molar masses below 2.1 kg mol⁻¹, i.e., a solute diameter of 2.4 nm, demonstrates a narrow pore size distribution. Using these results in combination with hindered transport models a pore diameter of 3.4 \pm 0.4 nm was estimated. The consistent rejection results between the parent copolymer and functionalized membranes clearly demonstrate that the nanoporous structure of the membranes was not affected during the functionalization process. As such, while there appears to be a change in permeability for all of the functionalized membranes compared to the unfunctionalized membrane, this is not due to a nanostructural change. Prior literature has shown that the grafting of zwitterionic brushes on hydrophobic surfaces can lead to increased permeability, 47,48' with the increase in permeability being attributed to the increased hydrophilicity of the membrane surface from the sulfonate group 48 as well as the ability of the zwitterion to increase the amount of free water at the membrane surface. 49,50 Swelling experiments (Figure S5) and contact angle measurements conducted with DI water (Figure S6) are consistent with the functionalized

membranes being more hydrophilic than the parent membrane. That is, upon functionalization, copolymer materials that were not constrained by a PVDF support exhibited 200—300% increases in their diameter.

Salt rejection experiments were conducted using 1 mM KCl, 1 mM K_2SO_4 , and 10 mM K_2SO_4 feed solutions. The percent rejection measured from these experiments is shown in Figure 4. Of the functionalized membranes, the full zwitterionic

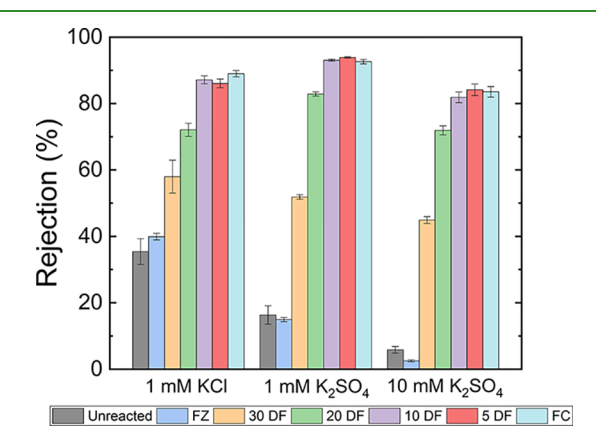


Figure 4. Ion rejection for unreacted, full zwitterionic (FZ), 30, 20, 10, and 5 s dual-functional (DF), and full charge (FC) membranes. The percent rejection was determined by taking the ratio of the K^+ ion concentration in the permeate to the feed. The K^+ concentrations were determined by using ICP-OES. The water flux was held constant at 5 L $m^{-2}\ h^{-1}$ by adjusting the applied pressure.

membrane exhibited the lowest rejection of salts with 40% rejection of KCl and 15% rejection of K_2SO_4 for the 1 mM feed solutions and no appreciable rejection of K_2SO_4 at 10 mM. These low rejection values were similar to the unreacted, parent membrane and can be attributed to the overall neutral zwitterionic functionality, which does not electrostatically repel dissolved ions from solution. The surface charge of the functionalized membranes was analyzed via streaming current analysis (Figure S7) to examine this hypothesis. The full zwitterionic and parent membranes possessed the lowest overall surface charge as evidence by a streaming current that was on average $4\times$ lower in magnitude than the current produced by the charge-functionalized membranes.

Because of the covalent attachment of sulfonic acid groups along the pore walls, the full charge and all dual-functional membranes showed similar streaming current values indicative of a negative surface charge. This negative surface charge manifests as the FC membrane exhibiting notably higher rejection values with 90% rejection of KCl and 93% rejection of K₂SO₄ for the 1 mM feed solutions and 84% rejection for the 10 mM K₂SO₄ feed solution. ^{52,53} This negative charge was present at pH values of 5.5 and 3, with >90% rejection of 1 mM K₂SO₄ achieved at both conditions (Figure S8). The FC membrane also exhibited low rejection of a divalent cation with 9% of the MgCl₂ from a 1 mM feed solution being rejected (Figure S8). The extent of dual functionality is highlighted by the ion rejection results for the series of DF membranes. Membranes with short initial reaction times, which have more negative charge content, resulted in higher rejection of the 1 mM KCl feed solution. The 5 DF, 10 DF, 20 DF, and 30 DF membranes rejected 86%, 87%, 72%, and 57% of the salt, respectively, from this feed solution. Here, the 5 DF and 10 DF membranes, demonstrate roughly equivalent rejection performance to that of the full charge membrane. There is a notable decrease in rejection for the membranes fabricated by using longer initial reactions, i.e., 20 DF and 30 DF samples, that appears to trend toward the rejection value of the full zwitterionic membrane. Similar trends were observed for the 1 and 10 mM K_2SO_4 feed solutions. At 1 mM, the rejection of K_2SO_4 is greater than KCl due to the stronger electrostatic repulsion of the divalent sulfate compared to the monovalent chloride, consistent with a Donnan exclusion mechanism that relies on electrostatic interactions between the membrane and dissolved salts. ⁵³ Additionally, K_2SO_4 rejection is lower at 10 mM due to the increased electrostatic screening (i.e., decreased Debye length) that results from the increase in ionic strength. ⁵⁴

The salt rejection experiments highlight that if designed appropriately, dual-functional membranes can achieve comparable salt rejection values relative to full charge membranes. Namely, using a short initial reaction with 3-(dimethylamino)-1-propyne leaves a majority of the underlying azide moieties available for further functionalization, which leads to membranes with similar incorporation of charged functionality and corresponding salt rejection properties. When the initial reaction occurs for an extended period of time, the reduction of available azides reduces the overall charge density of the membrane, and a corresponding decrease in rejection is observed for the 20 and 30 DF membranes. Balancing this consideration with the introduction of an effective antifouling top layer is needed to realize the utility of the DF membrane approach.

3.4. Quantifying Membrane Fouling Propensity. Bovine serum albumin (BSA) is a protein commonly used to characterize the fouling propensity of membranes. The Stokes radius of BSA, 3.5 nm, 55 is larger than the pore diameter of the copolymer membranes developed here, 3.4 ± 0.4 nm. As such, pore blockage and the formation of a cake layer on the top surface of the membrane are expected to be the primary mechanisms of fouling. These mechanisms will be driven by the attractive interactions between the foulants and the surface of the membrane. For the charge-functionalized membranes discussed here, the electrostatic interactions between BSA dissolved in solution and the membrane surface are critical to determining the magnitude of these interactions. One method for modulating these interactions is to examine the fouling profiles for solutions of varying pH. In particular, BSA has an isoelectric point at pH 4.7–4.9.⁵⁶ At this pH value, the protein has an equal balance of positive and negative charges, such that it is overall neutral. Below and above this pH value, the BSA molecules are positively and negatively charged, respectively.⁵ Based on this prior characterization, 0.5 g L⁻¹ BSA, 1 mM NaCl solutions adjusted to pH 3 or pH 4.7 were used for the initial series of fouling experiments. The pH 3 solution was chosen to maximize the electrostatic attraction between the positively charged foulant and the negatively charged membranes. The pH 4.7 solution was examined because it coincides with the isoelectric point of BSA.

The results from fouling experiments conducted at pH 3 are shown in Figure 5A. After the water flux stabilized at 5 L m⁻² h⁻¹, the BSA solution was introduced and the flux was monitored for 40 h. The FC membrane demonstrated the expected fouling performance for charged membranes. At a constant applied pressure of 2.06 bar (30 psi), a steady flux decline was observed, and after 40 h the FC membrane exhibited a 44% drop in normalized flux. Upon rinsing with DI

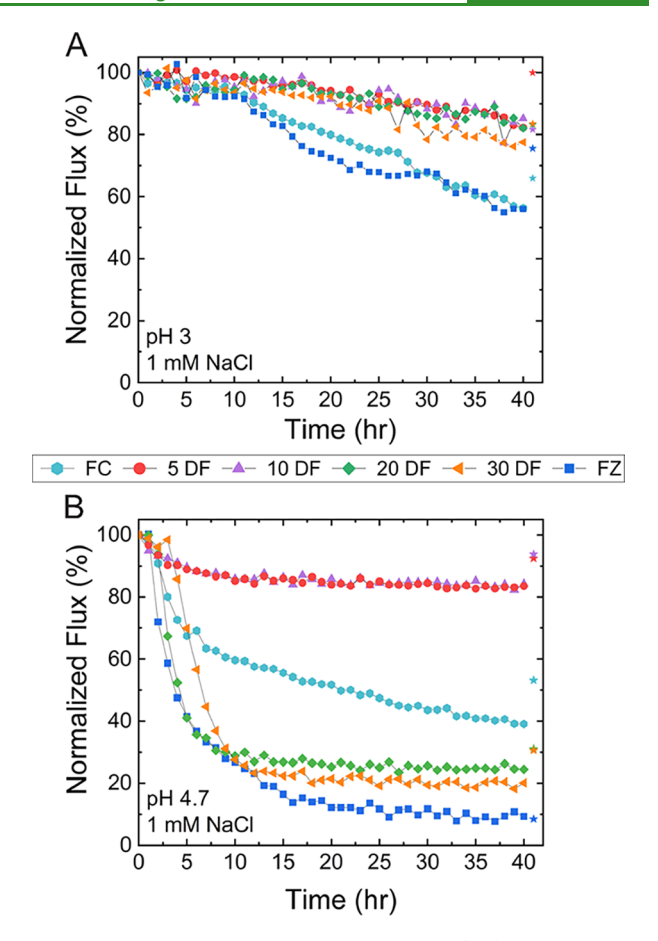


Figure 5. BSA fouling results for full zwitterionic (FZ), 30, 20, 10, and 5 s dual-functional (DF), and full charge (FC) membranes. A 0.5 g L^{-1} BSA solution with 1 mM NaCl at (A) pH 3 and (B) pH 4.7 was passed though the membrane for a period of 40 h. Prior to fouling, the flux was stabilized at 5 L m $^{-2}$ h $^{-1}$ by using an equivalent solution without foulant. This value was used for normalization of the flux recorded during the fouling experiment. After exposure to the foulant solution, the membrane was rinsed with DI water and the flux was tested again, with regained permeability shown as the star.

water, the flux through the membrane remained 35% lower than the initial flux. In other words, the FC membrane recovered to 65% of the initial flux after rinsing. In comparison, when the 5 DF membrane was exposed to the same BSA fouling solution, a flux decline of only 17% resulted after 40 h. Moreover, rinsing with DI water restored the water flux to 99% of its initial value. All of the other DF membranes showed nearly identical fouling performance with flux declines of 17%–20%, though upon rinsing were unable to recover the initial flux above 84%.

Surprisingly, the full zwitterionic membrane exhibited similar fouling performance to the full charge membrane. While a neutral, hydrophilic chemistry is one indicator of a surface that exhibits reduced fouling propensity, several additional parameters contribute to the overall fouling mechanism. For example, surface roughness is another major contributor toward membrane fouling whereby rough membranes exhibit higher fouling rates due to the accumulation of foulants within the valleys and troughs of the surface profile. The results from the swelling experiments suggest that the full zwitterionic membrane was most susceptible to swelling. While this resulted in an increase in diameter during the swelling experiments, the copolymer layer of membranes tested in

fouling experiments was restricted by the PVDF support layer which kept their diameter constant. Thus, the copolymer expansion is most likely translated to a change in surface structure and resulted in an increased roughness. This change in roughness was also noted as a visible change in surface profile of the FZ membrane. The 30 and 20 DF also demonstrated changes in surface roughness, but the 10 DF, 5 DF, and FC membranes did not (Figure S9). Attempts were made to collect atomic force microscopy (AFM) surface profiles (Figure S10), but high-resolution micrographs of the FZ membranes were difficult to obtain within a liquid environment. SEM micrographs of the dried surface were obtained and do appear to indicate a change in the surface structure (Figure S11).

The results from fouling experiments conducted using a 0.5 g L⁻¹ BSA, 1 mM NaCl feed solution at pH 4.7 are shown in Figure 5B. The FC membrane again showed high fouling rates, with a 60% decrease in flux after 40 h. Notably, the flux decline over time for the solution at pH 4.7 was different than that observed for the solution at pH 3. Instead of a steady decline in flux like that observed for the pH 3 solution, the pH 4.7 solution exhibited a severe drop in flux within the first 5 h, losing 30% of flux within this period, and a more gradual 30% loss in flux over the last 35 h. This sharp initial decline is consistent with fouling at the isoelectric point of BSA. 56 Namely, the electrostatic repulsion between BSA molecules in solution and BSA molecules on the fouled membrane surface is reduced under the pH 4.7 conditions, exacerbating the rate of fouling. 56,59 At a p \hat{H} of 3, as BSA begins to foul the surface, the electrostatic repulsions between the foulants on the membrane surface and the BSA molecules dissolved in solution slow the accumulation of a cake layer, leading to a more gradual decline in flux.⁵⁷ At a pH of 4.7, the initial deposition of BSA on the surface does not create a charged layer of foulants on the membrane surface that is capable of repelling additional BSA molecules in solution, resulting in a much more rapid initial flux decline. At longer times, the rate of fouling begins to decrease as the transport of water through the cake layer becomes the controlling resistance. 10 Eventually, a steady state is reached where the cake layer deposition is balanced with the shear force caused by stirring. 60 Rinsing the FC membrane with DI water recovered only 53% of the initial flux.

The 5 DF and 10 DF membranes each showed an overall flux reduction of 18%, equal to that of the pH 3 solution. The rate in which the fouling occurs differs though, with the pH 3 solutions having a gradual decrease compared to the more rapid decrease at pH 4.7. Following this decline, the normalized flux at pH 4.7 quickly reaches a steady value. Upon rinsing, the 5 DF and 10 DF membranes were able to regain 92% and 94% of the initial flux, respectively. The FZ, 20 DF, and 30 DF membranes also experience much more rapid flux decline relative to that observed at pH 3, with a 90% loss in flux observed for the FZ membrane. This observation correlates with the influence that surface roughness has on fouling. While a rougher surface will trap more foulants on the surface than a smooth membrane, at a pH of 3, the electrostatic repulsion of BSA in solution with that of BSA on the surface may reduce the overall rate of fouling. At a pH of 4.7, this repulsive interaction is dramatically reduced, and a rapid decline in flux is seen. Future efforts can design the copolymer material to better account for the impact of swelling on membrane performance. The present results do show that for a short exposure time the 5 DF and 10 DF membranes,

which demonstrated comparable ion rejection to the FC membranes, exhibit markedly improved fouling performance compared to the FC membranes.

The electrostatic interactions between BSA dissolved in solution and the membrane surface can also be modified by changing the ionic strength of the solution. This modification affects the characteristic distance over which charged solutes in solution interact with the surface, i.e., the Debye length. S9,61 Reducing the Debye length by increasing the salt concentration in solution has been shown to increase fouling due to the reduced electrostatic repulsion between BSA adsorbed on the surface and that in solution. Here, the effects of salt concentration on membrane fouling was analyzed by using solutions containing 0.5 g L⁻¹ BSA and salt concentrations of 1, 10, and 100 mM NaCl (Figure S12).

The FC membranes were tested with a foulant solution at pH 3, and the FZ membranes were tested at pH 4.7. These pH values were chosen as each corresponded to the most severe fouling observed at 1 mM NaCl for these two membranes. For the FC membrane at pH 3, increasing the salt concentration resulted in a decrease in fouling propensity. All three solutions resulted in similar fouling profiles for the first 10 h of testing, with the 1 mM solution beginning to have a more severe decrease in flux over the final 30 h. The final flux values for the FC membranes increased from 56% at 1 mM to 79% at 10 mM and finally 88% at 100 mM. This set of results is contrary to the idea that fouling becomes worse due to the increased shielding of electrostatic interactions at the membrane surface. While this shielding may reduce the repulsive interactions between BSA on the surface and BSA in solution, it may also shield the attractive interactions between the negatively charged surface and BSA, thereby reducing the fouling propensity. This trend has also been noticed when measuring the adsorption isotherms of BSA on poly(ether sulfone) ultrafiltration membranes.⁶²

The FZ membrane at pH 4.7 also experienced a decrease in fouling at increased salt concentrations. A reduced rate of initial fouling was seen at higher salt concentrations, with the flux for the 10 and 100 mM NaCl solution membranes remaining constant for the first 4 h exposed to BSA, while the 1 mM NaCl solution membrane had lost 57% of the initial flux at this same interval. The final flux values for FZ membranes fouled at 1, 10, and 100 mM were 9%, 24%, and 63% of the initial flux, respectively. As this solution is at the isoelectric point of BSA, the change in fouling is not attributed to shielding of the electrostatic charges, but rather a change in the structure of BSA. The compact BSA structure at the isoelectric point is attributed to the interactions between the oppositely charged functional groups within the BSA molecule. As the salt concentration increases, the added salt can begin to shield the interactions between the functional groups, resulting in a larger molecule. 56 As the FZ membrane has some surface roughness, a smaller molecule could be more easily trapped within the troughs and valleys of the surface, while a larger molecule may not be able to enter,⁵⁸ resulting in reduced fouling at higher salt concentrations.

Lastly, the 5 DF membrane was exposed to 100 mM NaCl solutions at both pH 3 and pH 4.7. In both instances, the 5 DF membrane experienced similar levels of flux decline independent of the NaCl concentration. There were some differences in fouling behavior though. For example, at pH 4.7, fouling for the 100 mM NaCl solution was delayed for the first 3 h of testing when compared to the 1 mM NaCl solution. The 100

mM NaCl solution membrane ended with a flux of 90% the initial flux, while the 1 mM NaCl solution membrane was slightly lower at 84%. At pH 3, the 5 DF membrane experienced a slightly greater decrease in flux for the 100 mM NaCl BSA solution. A similar steady decline in flux was seen for the 1 and 100 mM NaCl foulant solutions, except the 1 mM ended with 82% of the initial flux and the 100 mM ended with 67% of the initial flux. The ability of the 5 DF membranes to frequently exhibit lower fouling propensity relative to that of the FC membranes indicates that the controlled functionalization process is capable of creating the appropriate balance of antifouling and ion rejection moieties.

4. CONCLUSION

Multifunctional membranes, which exhibit high ion rejection by Donnan exclusion and antifouling characteristics, were fabricated by taking advantage of the rapid kinetics of the CuAAC reaction mechanism. Tailor-made copolymer membranes were exposed sequentially to two reactive solutions for controlled periods of time. A short initial reaction with 3-(dimethylamino)-1-propyne allowed the antifouling zwitterionic moieties to be localized near the top surface of the membrane without consuming all of the reactive azide moieties within the membrane. A subsequent reaction with negatively charged functional groups consumed the azide moieties underlying the antifouling layer to create the dual-functional membranes. These dual-functional membranes were able to achieve a comparable ion rejection performance to control membranes that were functionalized fully with negative charge. Moreover, the membrane with the dual-functional architecture exhibited notably lower fouling propensity relative to control membranes. These results demonstrate the potential that properly designing functionalization protocols to localize targeted functional groups within a membrane has for enhancing the performance of nanofiltration membranes. Moreover, the modular nature of the CuAAC and other click chemistry mechanisms offers a means by which to design and fabricate multifunctional, Janus membranes for a plethora of future applications.

ASSOCIATED CONTENT

5 Supporting Information

The Supporting Information is available free of charge at https://pubs.acs.org/doi/10.1021/acsami.0c03075.

Detailed experimental methodology regarding polymer synthesis and membrane fabrication, ¹H NMR spectra of copolymers, complete SEM-EDX images and line spectrum analysis, contact angle, membrane swelling, streaming current results, AFM, visual surface, and SEM surface images of functionalized membranes, and additional fouling experiments at increased salt concentrations (PDF)

AUTHOR INFORMATION

Corresponding Author

William A. Phillip — Department of Chemical and Biomolecular Engineering, University of Notre Dame, Notre Dame, Indiana 46556, United States; ⊚ orcid.org/0000-0001-8871-585X; Email: wphillip@nd.edu

Author

John R. Hoffman – Department of Chemical and Biomolecular Engineering, University of Notre Dame, Notre Dame, Indiana 46556, United States

Complete contact information is available at: https://pubs.acs.org/10.1021/acsami.0c03075

Notes

The authors declare no competing financial interest.

ACKNOWLEDGMENTS

This work was made possible with support from the National Science Foundation (NSF) through the Advanced Manufacturing Program (Award 1932206), and we appreciatively acknowledge this support. J.R.H. gratefully acknowledges support from the Center of Environmental Science and Technology (CEST)/Bayer Predoctoral Fellowship at the University of Notre Dame. We thank the Notre Dame Integrated Imaging Facility (NDIIF), the Center for Environmental Science and Technology (CEST), and the Materials Characterization Facility (MCF) at Notre Dame; portions of this research were performed with instruments at these facilities. We also thank Prof. Merlin Bruening for use of his contact angle goniometer.

REFERENCES

- (1) Eugene, E. A.; Phillip, W. A.; Dowling, A. W. Data Science-Enabled Molecular-to-Systems Engineering for Sustainable Water Treatment. *Curr. Opin. Chem. Eng.* **2019**, 26, 122–130.
- (2) Park, H. B.; Kamcev, J.; Robeson, L. M.; Elimelech, M.; Freeman, B. D. Maximizing the Right Stuff: The Trade-Off between Membrane Permeability and Selectivity. *Science* **2017**, *356*, 1138–1148.
- (3) Alvarez, P. J. J.; Chan, C. K.; Elimelech, M.; Halas, N. J.; Villagrán, D. Emerging Opportunities for Nanotechnology to Enhance Water Security. *Nat. Nanotechnol.* **2018**, *13*, 634–641.
- (4) Geise, G. M.; Park, H. B.; Sagle, A. C.; Freeman, B. D.; Mcgrath, J. E. Water Permeability and Water/Salt Selectivity Tradeoff in Polymers for Desalination. *J. Membr. Sci.* **2011**, *369*, 130–138.
- (5) Werber, J. R.; Deshmukh, A.; Elimelech, M. The Critical Need for Increased Selectivity, Not Increased Water Permeability, for Desalination Membranes. *Environ. Sci. Technol. Lett.* **2016**, *3*, 112–120
- (6) Werber, J. R.; Osuji, C. O.; Elimelech, M. Materials for Next-Generation Desalination and Water Purification Membranes. *Nat. Rev. Mater.* **2016**, *1*, 16018.
- (7) Sadeghi, I.; Kaner, P.; Asatekin, A. Controlling and Expanding the Selectivity of Filtration Membranes. *Chem. Mater.* **2018**, *30*, 7328–7354.
- (8) Qu, S.; Dilenschneider, T.; Phillip, W. A. Preparation of Chemically-Tailored Copolymer Membranes with Tunable Ion Transport Properties. ACS Appl. Mater. Interfaces 2015, 7, 19746—19754
- (9) Greenlee, L. F.; Lawler, D. F.; Freeman, B. D.; Marrot, B.; Moulin, P. Reverse Osmosis Desalination: Water Sources, Technology, and Today's Challenges. *Water Res.* **2009**, *43*, 2317–2348.
- (10) Guo, W.; Ngo, H. H.; Li, J. A Mini-review on Membrane Fouling. *Bioresour. Technol.* **2012**, 122, 27–34.
- (11) Asatekin, A.; Kang, S.; Elimelech, M.; Mayes, A. M. Anti-fouling Ultrafiltration Membranes Containing Polyacrylonitrile-graft-poly(ethylene oxide) Comb Copolymer Additives. *J. Membr. Sci.* **2007**, 298, 136–146.
- (12) Sun, Q.; Su, Y.; Ma, X.; Wang, Y.; Jiang, Z. Improved Antifouling Property of Zwitterionic Ultrafiltration Membrane Composed of Acrylonitrile and Sulfobetaine Copolymer. *J. Membr. Sci.* **2006**, 285, 299–305.

- (13) Rana, D.; Matsuura, T. Surface Modifications for Antifouling Membranes. *Chem. Rev.* **2010**, *110*, 2448–2471.
- (14) Ostuni, E.; Chapman, R. G.; Holmlin, R. E.; Takayama, S.; Whitesides, G. M. A Survey of Structure-property Relationships of Surfaces that Resist the Adsorption of Protein. *Langmuir* **2001**, *17*, 5605–5620
- (15) Yang, H. C.; Hou, J.; Chen, V.; Xu, Z. K. Janus Membranes: Exploring Duality for Advanced Separation. *Angew. Chem., Int. Ed.* **2016**, *55*, 13398–13407.
- (16) Yang, H.; Xie, Y.; Hou, J.; Cheetham, A.; Chen, V.; Darling, S. B. Janus Membranes: Creating Asymmetry for Energy Efficiency. *Adv. Mater.* **2018**, *30*, 1801495.
- (17) Zhou, H.; Guo, Z. Superwetting Janus Membranes: Focusing on Unidirectional Transport Behaviors and Multiple Applications. *J. Mater. Chem. A* **2019**, *7*, 12921–12950.
- (18) Song, H. M.; Chen, C.; Shui, X. X.; Yang, H.; Zhu, L.; Zeng, Z. X.; Xue, Q. J. Asymmetric Janus Membranes Based on In Situ Mussel-Inspired Chemistry for Efficient Oil/Water Separation. *J. Membr. Sci.* **2019**, *573*, 126–134.
- (19) Wu, M. B.; Yang, H. C.; Wang, J. J.; Wu, G. P.; Xu, Z. K. Janus Membranes with Opposing Surface Wettability Enabling Oil-to-Water and Water-to-Oil Emulsification. *ACS Appl. Mater. Interfaces* **2017**, *9*, 5062–5066.
- (20) Yang, J.; Li, H. N.; Chen, Z. X.; He, A.; Zhong, Q. Z.; Xu, Z. K. Janus Membranes with Controllable Asymmetric Configurations for Highly Efficient Separation of Oil-in-Water Emulsions. *J. Mater. Chem.* A 2019, 7, 7907–7917.
- (21) Guo, C.; Li, N.; Qian, X.; Shi, J.; Jing, M.; Teng, K.; Xu, Z. Ultra-thin Double Janus Nanofiltration Membrane for Separation of Li⁺ and Mg²⁺: 'Drag' Effect from Carboxyl-Containing Negative Interlayer. Sep. Purif. Technol. **2020**, 230, 115567.
- (22) Liu, S.; Wu, C.; Hung, W. S.; Lu, X.; Lee, K. R. One-step Constructed Ultrathin Janus Polyamide Nanofilms with Opposite Charges for Highly Efficient Nanofiltration. *J. Mater. Chem. A* **2017**, *S*, 22988–22996.
- (23) Li, C.; Li, X.; Du, X.; Tong, T.; Cath, T. Y.; Lee, J. Antiwetting and Antifouling Janus Membrane for Desalination of Saline Oily Wastewater by Membrane Distillation. ACS Appl. Mater. Interfaces 2019, 11, 18456–18465.
- (24) Ghaleni, M. M.; Al Balushi, A.; Kaviani, S.; Tavakoli, E.; Bavarian, M.; Nejati, S. Fabrication of Janus Membranes for Desalination of Oil- Contaminated Saline Water. *ACS Appl. Mater. Interfaces* **2018**, *10*, 44871–44879.
- (25) Zhou, S.; Liu, F.; Wang, J.; Lin, H.; Han, Q.; Zhao, S.; Tang, C. Y. Janus Membrane with Unparalleled Forward Osmosis Performance. *Environ. Sci. Technol. Lett.* **2019**, *6*, 79–85.
- (26) Li, Z.; Han, Y.; Wei, J.; Wang, W.; Cao, T.; Xu, S.; Xu, Z. Suppressing Shuttle Effect Using Janus Cation Exchange Membrane for High-Performance Lithium Sulfur Battery Separator. ACS Appl. Mater. Interfaces 2017, 9, 44776—44781.
- (27) Meng, N.; Lian, F.; Li, Y.; Zhao, X.; Zhang, L.; Lu, S.; Li, H. Exploring PVFM-Based Janus Membrane-Supporting Gel Polymer Electrolyte for Highly Durable Li O 2 Batteries. ACS Appl. Mater. Interfaces 2018, 10, 22237—22247.
- (28) Oh, Y. S.; Jung, G. Y.; Kim, J. H.; Kim, J. H.; Kim, S. H.; Kwak, S. K.; Lee, S. Y. Janus-Faced, Dual-Conductive/Chemically Active Battery Separator Membranes. *Adv. Funct. Mater.* **2016**, *26*, 7074–7082
- (29) Liu, Y.; Xiao, T.; Bao, C.; Fu, Y.; Yang, X. Fabrication of Novel Janus Membrane by Nonsolvent Thermally Induced Phase Separation (NTIPS) for Enhanced Performance in Membrane Distillation. *J. Membr. Sci.* **2018**, *563*, 298–308.
- (30) Zhang, W.; Li, X.; Qu, R.; Liu, Y.; Wei, Y.; Feng, L. Janus Membrane Decorated via a Versatile Immersion-spray Route: Controllable Stabilized Oil/water Emulsion Separation Satisfying Industrial Emission and Purification Criteria. *J. Mater. Chem. A* **2019**, 7, 4941–4949.

- (31) Yang, H. C.; Waldman, R. Z.; Wu, M. B.; Hou, J.; Chen, L.; Darling, S. B.; Xu, Z. K. Dopamine: Just the Right Medicine for Membranes. *Adv. Funct. Mater.* **2018**, 28, 1705327.
- (32) Yang, H. C.; Zhong, W.; Hou, J.; Chen, V.; Xu, Z. K. Janus Hollow Fiber Membrane with a Mussel-Inspired Coating on the Lumen Surface for Direct Contact Membrane Distillation. *J. Membr. Sci.* **2017**, *523*, 1–7.
- (33) Kasemset, S.; Wang, L.; He, Z.; Miller, D. J.; Kirschner, A.; Freeman, B. D.; Sharma, M. M. Influence of Polydopamine Deposition Conditions on Hydraulic Permeability, Sieving Coefficients, Pore Size and Pore Size Distribution for a Polysulfone Ultrafiltration Membrane. *J. Membr. Sci.* **2017**, *522*, 100–115.
- (34) Waldman, R. Z.; Yang, H. C.; Mandia, D. J.; Nealey, P. F.; Elam, J. W.; Darling, S. B. Janus Membranes via Diffusion-Controlled Atomic Layer Deposition. *Adv. Mater. Interfaces* **2018**, *5*, 1800658.
- (35) Tufani, A.; Ince, G. O. Protein Gating by Vapor Deposited Janus Membranes. J. Membr. Sci. 2019, 575, 126–134.
- (36) Dobosz, K. M.; Kuo-Leblanc, C. A.; Emrick, T.; Schiffman, J. D. Antifouling Ultrafiltration Membranes with Retained Pore Size by Controlled Deposition of Zwitterionic Polymers and Poly(ethylene glycol). *Langmuir* **2019**, *35*, 1872–1881.
- (37) Kolb, H. C.; Finn, M. G.; Sharpless, K. B. Click Chemistry: Diverse Chemical Function from a Few Good Reactions. *Angew. Chem., Int. Ed.* **2001**, *40*, 2004–2021.
- (38) Meldal, M.; Tomøe, C. W. Cu-catalyzed azide Alkyne cycloaddition. *Chem. Rev.* **2008**, *108*, 2952–3015.
- (39) Coceancigh, H.; Tran-Ba, K.; Siepser, N.; Baker, L. A.; Ito, T. Longitudinally Controlled Modification of Cylindrical and Conical Track-Etched Poly(ethylene terephthalate) Pores Using an Electrochemically Assisted Click Reaction. *Langmuir* **2017**, *33*, 11998–12006.
- (40) Hoffman, J. R.; Mikes, A. D.; Gao, F.; Phillip, W. A. Controlled Postassembly Functionalization of Mesoporous Copolymer Membranes Informed by Fourier Transform Infrared Spectroscopy. *ACS Appl. Polym. Mater.* **2019**, *1*, 2120–2130.
- (41) Zhang, Y.; Sargent, J. L.; Boudouris, B. W.; Phillip, W. A. Nanoporous Membranes Generated from Self-Assembled Block Polymer Precursors: Quo Vadis? *J. Appl. Polym. Sci.* **2015**, *132*, 1–17.
- (42) Wade, Jr., L. Organic Chemistry, 8th ed.; Pearson Prentice Hall: Upper Saddle River, NJ, 2012.
- (43) Meireles, M.; Bessieres, A.; Rogissart, I.; Aimar, P.; Sanchez, V. An Appropriate Molecular Size Parameter for Porous Membranes Calibration. *J. Membr. Sci.* **1995**, *103*, 105–115.
- (44) Zeman, L.; Wales, M. Steric Rejection of Polymeric Solutes by Membranes with Uniform Pore Size Distribution. *Sep. Sci. Technol.* **1981**, *16*, 275–290.
- (45) Bowen, W.; Mukhtar, H. Characterisation and Prediction of Separation Performance of Nanofiltration Membranes. *J. Membr. Sci.* **1996**, *112*, 263–274.
- (46) Déon, S.; Koubaa, Z.; Korzhova, E.; Airoudj, A.; Fievet, P.; Roucoules, V. Understanding the Impact of Poly(allylamine) Plasma Grafting on the Filtration Performances of a Commercial Polymeric Membrane. *Sep. Purif. Technol.* **2019**, *212*, 30–39.
- (47) Davenport, D. M.; Lee, J.; Elimelech, M. Efficacy of Antifouling Modification of Ultrafiltration Membranes by Grafting Zwitterionic Polymer Brushes. *Sep. Purif. Technol.* **2017**, *189*, 389–398.
- (48) Guo, Y. S.; Mi, Y. F.; Ji, Y. L.; An, Q. F.; Gao, C. J. One-Step Surface Grafting Method for Preparing Zwitterionic Nanofiltation Membrane via In Situ Introduction of Initiator in Interfacial Polymerization. ACS Appl. Polym. Mater. 2019, 1, 1022–1033.
- (49) An, Q. F.; Sun, W. D.; Zhao, Q.; Ji, Y. L.; Gao, C. J. Study on a Novel Nanofiltration Membrane Prepared by Interfacial Polymerization with Zwitterionic Amine Monomers. *J. Membr. Sci.* **2013**, *431*, 171–179.
- (50) Schlenoff, J. B. Zwitteration: Coating Surfaces with Zwitterionic Functionality to Reduce Nonspecific Adsorption. *Langmuir* **2014**, *30*, 9625–9636.
- (51) Georgiev, G. S.; Kamenska, E. B.; Vassileva, E. D.; Kamenova, I. P.; Georgieva, V. T.; Iliev, S. B.; Ivanov, I. A. Self-assembly, Anti

- Polyelectrolyte Effect, and Nonbiofouling Properties of Polyzwitterions. *Biomacromolecules* **2006**, *7*, 1329–1334.
- (52) Donnan, F. G. The Theory of Membrane Equilibria. *Chem. Rev.* **1924**, *1*, 73–90.
- (53) Yaroshchuk, A. Non-steric Mechanisms of Nanofiltration: Superposition of Donnan and Dielectric Exclusion. *Sep. Purif. Technol.* **2001**, *22*, 143–158.
- (54) Kohonen, M. M.; Karaman, M. E.; Pashley, R. M. Debye Length in Multivalent Electrolyte Solutions. *Langmuir* **2000**, *16*, 5749–5753.
- (55) Persson, A.; Jönsson, A. S.; Zacchi, G. Transmission of BSA During Cross-flow Microfiltration: Influence of pH and Salt Concentration. *J. Membr. Sci.* **2003**, 223, 11–21.
- (56) Mo, H.; Tay, K. G.; Ng, H. Y. Fouling of Reverse Osmosis Membrane by Protein (BSA): Effects of pH, Calcium, Magnesium, Ionic Strength and Temperature. *J. Membr. Sci.* **2008**, *315*, 28–35.
- (57) Ang, W.; Elimelech, M. Protein (BSA) Fouling of Reverse Osmosis Membranes: Implications for Wastewater Reclamation. *J. Membr. Sci.* **2007**, *296*, 83–92.
- (58) Vrijenhoek, E. M; Hong, S.; Elimelech, M. Influence of Membrane Surface Properties on Initial Rate of Colloidal Fouling of Reverse Osmosis and Nanofiltration Membranes. *J. Membr. Sci.* **2001**, *188*, 115–128.
- (59) Del La Casa, E. J.; Guadix, A.; Ibáñez, R.; Camacho, F.; Guadix, E. M. A Combined Fouling Model to Describe the Influence of the Electrostatic Environment on the Cross-flow Microfiltration of BSA. *J. Membr. Sci.* **2008**, *318*, 247–254.
- (60) Shirazi, S.; Lin, C. J.; Chen, D. Inorganic Fouling of Pressure-driven Membrane Processes A Critical Review. *Desalination* **2010**, 250, 236–248.
- (61) Israelachvili, J. N. Intermolecular and Surface Forces, 3rd ed.; Academic Press: New York, 2010.
- (62) Salgın, S.; Takaç, S.; Özdamar, T. Adsorption of Bovine Serum Albumin on Polyether Sulfone Ultrafiltration Membranes: Determination of Interfacial Interaction Energy and Effective Diffusion Coefficient. J. Membr. Sci. 2006, 278, 251–260.